

Optimizing The Cut And Count Method In Phenomenological Studies

BARADHWAJ COLEPPA,^{1,*} GOKUL B. KRISHNA^{b,1,†} AGNIVO SARKAR,^{2,§} and SUJAY SHIL^{3,¶}

¹*Indian Institute of Technology Gandhinagar, Gujarat 382055, India.*

²*Regional Centre for Accelerator-based Particle Physics, Harish-Chandra Research Institute, Prayagraj (Allahabad) 211019, India*

³*Instituto de Física, Universidade de São Paulo, R. do Matão 1371, 05508-090 São Paulo, Brazil*

We introduce an optimization technique to discriminate signal and background in any phenomenological study based on the cut and count-based method. The core ideas behind this technique are the introduction of a ranking scheme that can quantitatively assess the relative importance of various observables involved in a new physics process, and a more methodical way of choosing what cuts to impose. The technique is an iterative process that works with the help of the MadAnalysis5 interface. Working in the context of a BSM (Beyond Standard Model) scenario where we carry out a signal search of singly charged Higgs in the context of the Two Higgs Doublet Model (2HDM), we demonstrate how automating the cut and count process in this specific way results in an enhanced discovery potential compared with the more traditional way of imposing cuts.

I. INTRODUCTION

It is by now firmly established that the Standard Model (SM) [1–3] of particle physics, while an enormously successful theory whose predictions have been tested to very good accuracy in various colliders over the years, needs to be supplanted with new dynamics at the TeV scale. With the advent of the Large Hadron Collider (LHC), we now have a testing ground for many of these so-called “Beyond the SM” (BSM) avenues. Typically one expects some new resonances at the TeV scale to show up in high energy collisions - however, such a discovery has thus far eluded us. This has prompted both experimentalists and theorists to employ increasingly sophisticated approaches toward phenomenological analyses with various machine learning (ML) and deep learning algorithms [4, 5] now at the forefront of particle physics research. The reason for this is of course clear - the traditional “bump hunting” searches, while successful in the past, might need to be replaced for a more thorough search. In this work, we offer an alternative strategy - while still employing the cut-based methodology, we aim to demonstrate that suitably automating this process can lead to significant enhancements in our search efficiency and thus might lead to a better discovery potential of new physics.

The study of BSM physics has been structured and scrutinized in many ways over the decades. The standard practice amongst phenomenologists now is a simulation tool such as MadGraph [6] for event generation which is compatible with FeynRules [7] for new physics model implementation. Also, to consider realistic collider situations, one has to cascade the parton level process from MadGraph to PYTHIA6 [8] for jet showering and Delphes3 [9] for detector-level simulations. The analysis of collision events proceeds via MadAnalysis5 [10] which is a framework for phenomenological analysis that handles data structures and facilitates effective analysis of particle physics scattering experiments through a user-friendly interface. which provides the user with normalized observable distributions. The “cut and count” strategy then relies on looking at the distributions and imposing suitable cuts to improve the signal over background significance. However, this practice of the cut-and-count method is ignorant of *how implementing a cut on a particular distribution will affect the remaining observable distributions*. While this might not be a huge disadvantage in say a $2 \rightarrow 2$ process with not a lot of SM background, for more complicated decay chains, one would need to understand the interplay between the various kinematic quantities. As we will demonstrate, we can optimize the cut and count methodology by formulating an iterative process with a suitably designed set of techniques to optimize the cut-flow.

While high-performing deep learning algorithms display superior capabilities in discrimination tasks [11, 12], the intricate structure of these data models is notably complex. This complexity arises from many tunable parameters and the numeric nature of the optimization process, posing challenges to a comprehensive understanding of its physical nature. Some studies have directed their attention towards exploring the phenomenologically relevant characteristics of neural networks in terms of interpretability [13, 14], and there are issues regarding uncertainty quantification [15, 16] as well. Our present study is not intended as a substitution for ML techniques; it is presented as a methodology which

^b corresponding author

* baradhwaj@iitgn.ac.in

† gokulb@iitgn.ac.in

§ agnivosarkar@hri.res.in

¶ sujayshil1@gmail.com

gives phenomenologically interpretable results and improves the sequential cut and count techniques for challenging final states at the LHC where traditional methods might not isolate the signals efficiently.

This paper is organized as follows: we begin by briefly explaining the BSM model that we will use as an example for illustrating the methodology in [section II](#) and outline the data domain that we are going to use to implement the algorithm. In [section III](#), we detail the development of the algorithm - this forms the crux of the paper wherein we present and explain a flowchart representing the execution of the various steps involved in the method. Finally, the benefits of adopting such a method - and its shortcomings - are discussed in [section IV](#).

II. SET-UP AND EXAMPLE

Our goal in this section is to lay out the example that we will use to illustrate our methodology and the underlying model details. Specifically, we choose to study charged Higgs pair production in the Type III¹ Two Higgs Doublet Model (2HDM) [17]. In the 2HDM, the SM scalar sector is extended by an additional scalar doublet Φ , which is charged under the electroweak gauge group $SU(2)_L \times U(1)_Y$ with hypercharge $Y = 1$. We lay out the basics of the scalar sector of the model that is directly relevant to our analysis and proceed to the phenomenological process of interest.

A. Model Set Up

In this section, we will present a brief review of the 2HDM model. For a more detailed description of the model, the interested reader is invited to consult Refs.[17, 18]. For our purpose here, we will concentrate on the scalar sector of the model. We begin, in Eq. 1, with the most general scalar potential of the theory which remains invariant under the SM gauge group $SU(2)_L \times U(1)_Y$.

$$\begin{aligned} V_H = & m_{11}^2 \Phi_1^\dagger \Phi_1 + m_{22}^2 \Phi_2^\dagger \Phi_2 - \left(m_{12}^2 \Phi_1^\dagger \Phi_2 + \text{h.c.} \right) + \frac{1}{2} \lambda_1 \left(\Phi_1^\dagger \Phi_1 \right)^2 + \frac{1}{2} \lambda_2 \left(\Phi_2^\dagger \Phi_2 \right)^2 \\ & + \lambda_3 \left(\Phi_1^\dagger \Phi_1 \right) \left(\Phi_2^\dagger \Phi_2 \right) + \lambda_4 \left(\Phi_1^\dagger \Phi_2 \right) \left(\Phi_2^\dagger \Phi_1 \right) \\ & + \left(\frac{1}{2} \lambda_5 \left(\Phi_1^\dagger \Phi_2 \right)^2 + \text{h.c.} \right) + \left(\lambda_6 \left(\Phi_1^\dagger \Phi_1 \right) \left(\Phi_1^\dagger \Phi_2 \right) + \lambda_7 \left(\Phi_2^\dagger \Phi_2 \right) \left(\Phi_1^\dagger \Phi_2 \right) + \text{h.c.} \right), \end{aligned} \quad (1)$$

where we have denoted the two $SU(2)_L$ doublets by Φ_1 and Φ_2 . Implementing the hermiticity condition, one can realize that m_{11}^2 , m_{22}^2 , and λ_i ($i = 1$ to 4) are real parameters. In contrast, m_{12}^2 and λ_i ($i = 5$ to 7) can, in general, be complex parameters. The presence of complex parameters can give rise to CP as well as charge violating minima which in turn hint upon interesting new physics scenarios. However, for the present purpose we will ignore these possibilities and impose a few conditions to simplify the above potential. We begin with the assumption that CP is conserved in the scalar sector. As a result, all the quartic terms which are odd powers of either of the scalar doublet drop out. Furthermore, we will assume all the scalar parameters in the potential are real. Under these conditions, Eqn. 1 takes the following form:

$$\begin{aligned} V_H = & m_{11}^2 \Phi_1^\dagger \Phi_1 + m_{22}^2 \Phi_2^\dagger \Phi_2 - \left(m_{12}^2 \Phi_1^\dagger \Phi_2 + \text{h.c.} \right) + \frac{1}{2} \lambda_1 \left(\Phi_1^\dagger \Phi_1 \right)^2 + \frac{1}{2} \lambda_2 \left(\Phi_2^\dagger \Phi_2 \right)^2 \\ & + \lambda_3 \left(\Phi_1^\dagger \Phi_1 \right) \left(\Phi_2^\dagger \Phi_2 \right) + \lambda_4 \left(\Phi_1^\dagger \Phi_2 \right) \left(\Phi_2^\dagger \Phi_1 \right) + \left(\frac{1}{2} \lambda_5 \left(\Phi_1^\dagger \Phi_2 \right)^2 + \text{h.c.} \right). \end{aligned} \quad (2)$$

Both these doublets acquire vacuum expectation values (*vevs*) given by $\langle \Phi_1 \rangle = v_1$ and $\langle \Phi_2 \rangle = v_2$, and thus engineer the electroweak symmetry breaking (EWSB) $SU(2)_L \times U(1)_Y \rightarrow U(1)_{\text{EM}}$. The explicit form of these doublets can be written as:

$$\Phi_i = \begin{pmatrix} \phi_i^+ \\ \frac{(\rho_i + v_1 + i\eta_1)}{\sqrt{2}} \end{pmatrix} \quad i = 1, 2. \quad (3)$$

¹ In the case of Type III 2HDM, the quark sector receives mass after both the scalar doublets Φ_1 and Φ_2 acquire *vevs*. As a consequence, this model can potentially generate flavour changing neutral currents at the tree level. A detailed discussion this can be found in Ref.[17]. We point out at this stage that in the upcoming phenomenology sections, we have chosen the benchmark point for our study that is compatible with flavour constraints.

One can see by direct inspection that both these doublets contain total eight total degrees of freedom (*d.o.f*) (ϕ_i^\pm, ρ_i , and η_i). After EWSB, three linear combinations of three of these *d.o.f*'s - the massless Goldstone modes - get absorbed by the SM electroweak gauge bosons W^\pm and Z rendering them massive. Thus, the scalar spectrum contains five physical Higgs bosons - a pair of charged Higgs bosons H^\pm (with mass m_{H^\pm}), a CP-odd scalar A (with mass m_A), and two CP-even scalars $\{h, H\}$ (with mass m_h and m_H respectively). We can see the spectrum emerge in the following way: the mass matrix corresponding to the charged scalars can be read off from V_H by collecting all the quadratic terms in fields and takes the following form:

$$\mathcal{L}_{\text{charged}} = (m_{12}^2 (\lambda_4 + \lambda_5) v_1 v_2) \begin{bmatrix} \phi_1^- & \phi_2^- \end{bmatrix} \begin{bmatrix} \frac{v_2}{v_1} & -1 \\ -1 & \frac{v_1}{v_2} \end{bmatrix} \begin{bmatrix} \phi_1^- \\ \phi_2^- \end{bmatrix}. \quad (4)$$

The determinant of the above 2×2 square matrix is zero. This signifies that at least one of the eigenvalues correspond to that matrix must be zero. The eigenvector correspond to the zero eigenvalue is identified as the charged Goldstone mode G^\pm which gets eaten up by the W^\pm boson. On other hand, the physical state correspond to the non zero eigenvalue is identified as H^\pm state with mass

$$m_{H^\pm} = \left[\frac{m_{12}^2}{v_1 v_2} - \lambda_4 - \lambda_5 \right]^{\frac{1}{2}} \sqrt{(v_1^2 + v_2^2)}. \quad (5)$$

Similarly, collecting the relevant quadratic terms one can write down the mass matrix correspond to CP-odd scalars:

$$\mathcal{L}_{\text{CP-odd}} = \frac{m_A^2}{v_1^2 + v_2^2} \begin{bmatrix} \eta_1 & \eta_2 \end{bmatrix} \begin{bmatrix} v_2^2 & -v_1 v_2 \\ -v_1 v_2 & v_1^2 \end{bmatrix} \begin{bmatrix} \eta_1 \\ \eta_2 \end{bmatrix}. \quad (6)$$

Here also, one of the eigenvalue would be zero which is associated with the neutral goldstone mode G^0 . The non zero eigenvalue represents the pseudo-scalar boson with mass

$$m_A = \left[\frac{m_{12}^2}{v_1 v_2} - \lambda_5 \right]^{\frac{1}{2}} \sqrt{(v_1^2 + v_2^2)}. \quad (7)$$

Finally, we turn to the mass matrix for the CP-even scalars - this can again be written down by straightforward inspection of the potential collecting quadratic terms in the ρ fields:

$$\begin{aligned} \mathcal{L}_{\text{mass}}^{\text{CP-even}} &= \begin{bmatrix} \rho_1 & \rho_2 \end{bmatrix} \begin{bmatrix} \mathcal{M}_{11} & \mathcal{M}_{12} \\ \mathcal{M}_{12} & \mathcal{M}_{22} \end{bmatrix} \begin{bmatrix} \rho_1 \\ \rho_2 \end{bmatrix} \\ &= \begin{bmatrix} \rho_1 & \rho_2 \end{bmatrix} \begin{bmatrix} m_{12}^2 \frac{v_2}{v_1} + \lambda_1 v_1^2 & -m_{12}^2 + \lambda_{345} v_1 v_2 \\ -m_{12}^2 + \lambda_{345} v_1 v_2 & m_{12}^2 \frac{v_2}{v_1} + \lambda_2 v_2^2 \end{bmatrix} \begin{bmatrix} \rho_1 \\ \rho_2 \end{bmatrix} \end{aligned} \quad (8)$$

In general, the above mass matrix has two non-zero eigenvalues which can be expressed as

$$\begin{aligned} m_H^2 &= \frac{1}{2} \left[\mathcal{M}_{11} + \mathcal{M}_{22} + \sqrt{(\mathcal{M}_{11} - \mathcal{M}_{22})^2 + \mathcal{M}_{12}^2} \right], \\ m_h^2 &= \frac{1}{2} \left[\mathcal{M}_{11} + \mathcal{M}_{22} - \sqrt{(\mathcal{M}_{11} - \mathcal{M}_{22})^2 + \mathcal{M}_{12}^2} \right]. \end{aligned} \quad (9)$$

Hereafter we assume $m_h < m_H$ and the CP-even state h with the mass m_h can be identified with the SM-like 125 GeV Higgs boson² discovered at the LHC. One can also define two parameters $\tan \beta$ and α using the *vev*'s and the scalar parameters:

$$\tan \beta = \frac{v_2}{v_1}, \quad \tan 2\alpha = \frac{2\mathcal{M}_{12}}{\mathcal{M}_{11} - \mathcal{M}_{22}}. \quad (10)$$

With these parameters, one can write down the relations between the gauge basis and the mass basis of the scalar fields.

$$\begin{aligned} \begin{bmatrix} G^\pm \\ H^\pm \end{bmatrix} &= \begin{bmatrix} \cos \beta & \sin \beta \\ -\sin \beta & \cos \beta \end{bmatrix} \begin{bmatrix} \phi_1^\pm \\ \phi_2^\pm \end{bmatrix} \\ \begin{bmatrix} G^0 \\ A \end{bmatrix} &= \begin{bmatrix} \cos \beta & \sin \beta \\ -\sin \beta & \cos \beta \end{bmatrix} \begin{bmatrix} \eta_1 \\ \eta_2 \end{bmatrix} \\ \begin{bmatrix} H \\ h \end{bmatrix} &= \begin{bmatrix} \cos \alpha & \sin \alpha \\ -\sin \alpha & \cos \alpha \end{bmatrix} \begin{bmatrix} \rho_1 \\ \rho_2 \end{bmatrix} \end{aligned} \quad (11)$$

² Even though a bit more constrained, 2HDM also allows the identification of the heavier of the two as the 125 GeV SM-like Higgs, thus making the other Higgs lighter. We do not explore this possibility in this paper.

ZH^+H^-	$-ie \cot \theta_W [P_{h^+}^\mu + P_{h^-}^\mu]$	[19]
γH^+H^-	$-ie [P_{h^+}^\mu + P_{h^-}^\mu]$	[19]
H^+W^-A	$-\frac{ig}{2}$	[20]
Abb	$-i \frac{m_b}{v} [-\cot \beta \sin(\beta - \alpha) + \cos(\beta - \alpha)]$	[20]

TABLE I: The vertices in the 2HDM relevant for our study. Here, θ_W is the weak mixing angle, $P_{h^\pm}^\mu$ is the momentum of h^\pm , m_b is the b-quark mass, and g is the $SU(2)_L$ coupling.

In computing all relevant couplings and studying the phenomenology, we use the above definitions of the mass eigenstates. Before closing this section, we present the relevant couplings in Table. I that will play a central role in the signal topology we will soon discuss. We point out that the vertices responsible for the charged Higgs pair production is independent of any new physics parameters. On top of that, the coupling responsible for the $H^\pm \rightarrow W^\pm A$ decay strictly depends on the $SU(2)_L$ gauge coupling. As a result, the relevance of this signal is not only restricted to 2HDM but a larger class of scalar extended BSM scenarios which can in principle allow the kind of signal we will study. Furthermore, comparing Eq. 5 and Eq. 7, one can realise that the mass gap between the m_{H^\pm} and m_A is controlled by the scalar parameter λ_4 . With the relevant pieces of the model in place, we now turn to the specific new physics process that we will use to illustrate our methodology.

B. Illustrative Process

In order to demonstrate the efficacy of our algorithm, we will study the pair production of charged Higgs bosons in the 2HDM with their subsequent decay into AW^\pm with the A 's decaying to $b\bar{b}$ and the W 's decaying leptonically:

$$pp \rightarrow H^+H^- \rightarrow W^+W^-AA \rightarrow 4b + 2l + \cancel{E}_T$$

This signal is quite challenging to reconstruct, given its small cross-section compared to the SM backgrounds and a complex final state topology. For the purposes of this study, we fix the mass of the charged Higgs boson at 450 GeV. We have also assigned the masses of the CP-even Higgs $m_H = 250$ GeV and the CP-odd pseudoscalar Higgs $m_A = 350$ GeV for the purpose of this study, apart from fixing the charged Higgs mass $m_{H^\pm} = 450$ GeV. This choice of charged Higgs mass, $H^\pm = 450$ GeV, remains viable in several popular beyond-Standard-Model (BSM) scenarios [17]. This mass point has not yet been ruled out in the $H^\pm \rightarrow \tau^\pm \nu$ channel by ATLAS [21] and CMS [22], nor in the $H^\pm \rightarrow tb$ channel by ATLAS [23] and CMS [22]. Furthermore, updated information regarding the Two-Higgs-Doublet Model fits [24] supports this scenario. Moreover, this mass value lies within a range of particular interest for future colliders, such as the High-Luminosity LHC (HL-LHC).

We first present a conventional cut and count analysis with a luminosity of 3000 fb^{-1} . The initial preselection cuts include $N(l) \geq 2$ and $N(b) \geq 4$, and $\Delta R(ll)$ and $\Delta R(bb) > 0.4$ to effectively separate all pairs of leptons and b-quarks. Examining the final state topology, the major SM backgrounds considered for this process are $t\bar{t} + jets$, $VV + jets$, and those with subdominant contributions from $VVV + jets$. Moreover, we have also included Vh , $t\bar{t}h$ as essential part of the SM background. We have compiled a set of 29 observables for the analysis.³ which can, in principle, aid in discriminating signal from background. These are

1. $P_T(\ell_1)$, 2. $P_T(\ell_2)$, 3. $P_T(b_1)$, 4. $P_T(b_2)$, 5. $P_T(b_3)$, 6. $P_T(b_4)$, 7. $\eta(\ell_1)$, 8. $\eta(\ell_2)$, 9. $\eta(b_1)$, 10. $\eta(b_2)$, 11. $\eta(b_3)$, 12. $\eta(b_4)$, 13. $\Delta R(\ell_1, \ell_2)$, 14. $\Delta R(b_1, b_2)$, 15. $\Delta R(b_1, b_3)$, 16. $\Delta R(b_1, b_4)$, 17. $\Delta R(b_2, b_3)$, 18. $\Delta R(b_2, b_4)$, 19. $\Delta R(b_3, b_4)$, 20. THT , 21. \cancel{E}_T , 22. $M(\ell_1, \ell_2)$, 23. $M(b_1, b_2)$, 24. $M(b_1, b_3)$, 25. $M(b_1, b_4)$, 26. $M(b_2, b_3)$, 27. $M(b_2, b_4)$, 28. $M(b_3, b_4)$, 29. $M(\ell_1, \ell_2, b_1, b_2, b_3, b_4)$.

The initial distributions acquired following the application of preselection cuts are depicted in Figure 1. By examining these distributions, one can straightforwardly determine the selection cuts that maximizes the signal-to-background ratio. We have established a set of selection criteria from intuition gained from the initial observable distribution and the result of this traditional cut and count analysis is presented in Table II - as one can see, this methodology does not produce a large enough significance (defined consistently throughout the text as $\sigma = \frac{S}{\sqrt{S+B}}$ where S and B refer to the number of signal and background events respectively) because one cannot eliminate the background effectively without incurring the large cost of diminishing the signal cross-section as well.⁴

³ While this might be exhaustive for a traditional cut and count analysis, it will prove effective to start with a maximal set for the algorithm which will be designed in the next section.

⁴ Introducing additional cuts in this example does not help much, and the significance hovers around the 1σ mark.

In addition to purely statistical uncertainties, there could be systematic uncertainties as well. We compute the significance calculation in the presence of systematic uncertainties (computed as $x\%$ of the background cross-section) as in Equation 12 [25, 26]. In this formula, S and B represent the number of signal and background events at a given instance. We have taken $x = 0.1$, corresponding to a 10% systematic uncertainty. This quantity has also been evaluated at the end of all the cutflow charts obtained in our study and displayed in Tables II, IV and V.

$$Z = \sqrt{2} \left[(S+B) \ln \left[\frac{(S+B)(B+\Delta_B^2)}{B^2 + (S+B)\Delta_B^2} \right] - \frac{B^2}{\Delta_B^2} \ln \left[1 + \frac{\Delta_B^2 S}{B(B+\Delta_B^2)} \right] \right]^{\frac{1}{2}} \quad \text{with} \quad \Delta_B = xB. \quad (12)$$

We note here that statistical significance is calculated either as $\sigma = \frac{S}{\sqrt{S+B}}$ (as we have done here), or in the limit that the number of background events is larger than the signal (which is often the case in particle physics experiments), as $\sigma = \frac{S}{\sqrt{B}}$. The connection between this significance with purely statistical errors, and the one in Eqn. 12 with the systematics accounted for can be understood as follows: in the limit that there are no systematic uncertainties, i.e., $\Delta_B = 0$, Eqn. 12 reduces to $Z = \sqrt{2} \left[(S+B) \ln \left(\frac{S+B}{B} \right) - S \right]$. In the limit that $S \ll B$, we can expand the logarithm and see that this reduces to S/\sqrt{B} . Thus, the formula $\sigma = S/\sqrt{B}$ is strictly only true if there are no systematic uncertainties, and the background cross-section is larger than that of the signal. We have displayed our results both for this limit (denoted as σ) and for the significance estimated in the more general way including both statistical and systematic uncertainties (denoted as Z).

Since we defined the objects that calculate significance and uncertainty, the observables identified as promising candidates for selection cuts, based on our inspection, are $P_T(b_1)$, $P_T(b_2)$, H_T , and $M(\ell_1, \ell_2, b_1, b_2, b_3, b_4)$. These observables exhibit better signal-to-background separation compared to others. Following the conventional cut-and-count strategy, we have implemented the set of selection cuts listed in Table II.

Having set up the premise and the model framework within which we will work, we now move on to the design of the algorithm and discuss various aspects of it.

-	N_{signal}	N_{BG}	σ	Z
Preselection	158.8	153612	0.405	0.010
$PT(b_1) > 175$	143	32564	0.791	0.043
$PT(b_2) > 125$	131.4	16394	1.022	0.079
$H_T > 600$	130.5	15078	1.058	0.086
$M(\ell_1, \ell_2, b_1, b_2, b_3, b_4) > 600$	129.7	14957	1.056	0.086

TABLE II: Cut Flow chart implemented by inspection of the distributions in Figure 1.

III. DEVELOPMENT OF THE ALGORITHM

The technique we will develop in this section is a coalition of a few simple concepts. The first step in any conventional analysis is to begin by choosing the most “obvious” variable to put a cut on - oftentimes, this happens to be one the p_T ’s of the jets or leptons. The subsequent steps might identify more variables that could aid in the isolation of the signal from the background usually culminating in a cut on the invariant mass of the heavy particle whose discovery is sought. While this is by no means standard, it does form a reasonable representation of the cut and count method. What we aim to do here is to optimize this method by answering the following questions in a quantitative manner:

1. How does one choose the kinematic variable that will maximally aid S vs B?
2. Having identified the variable, how does one choose the exact cut that will maximally isolate the signal?
3. How does one continue the process taking care to ensure the significance increases with every step?

We will begin by introducing relevant quantities of interest that will simultaneously answer these questions.

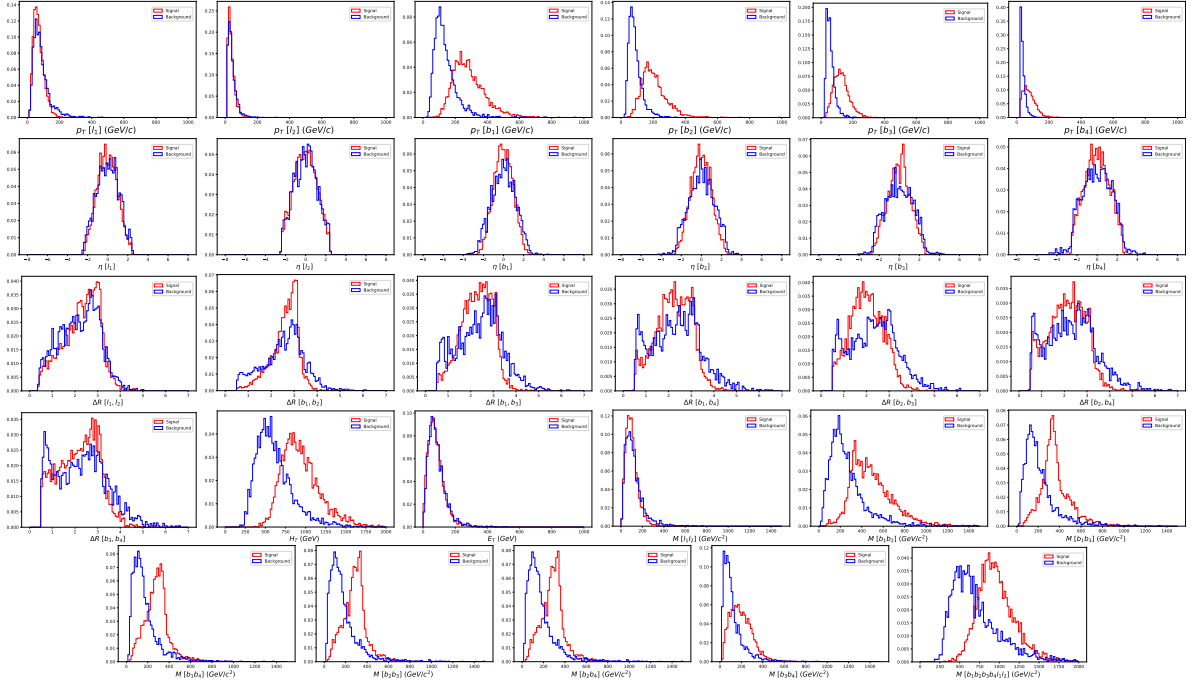


FIG. 1: The normalized distributions of the 29 observables mentioned in the text after the pre-selection cuts.

A. The Area Parameter and Ranking

As we mentioned, we start our analysis from the normalized distributions obtained from the MadAnalysis5 - after the preselection cuts mentioned earlier - to initiate the process of identifying variables. Even though there are numerous statistical metrics available for evaluating the separation between two normalized distributions (specifically, the signal and background distributions in our case), commonly used in various applications such as Bhattacharyya Distance [27] and Kullback-Leibler Divergence [28] among others, we introduce a novel parameter termed the **Area Parameter** (AP). The AP serves as a metric to quantify the extent of separation between the signal and background distributions. To compute the AP, we initially transform the normalized distribution, which is a probability distribution, into a cumulative distribution function (CDF). The CDF of a real variable Y is defined as follows:

$$F_Y(y) = P(Y \leq y), \quad (13)$$

i.e., the CDF is a measure of the probability that the value of the variable Y is less than or equal to y . Thus the CDF is, by definition, a curve that starts from zero and asymptotes to one, i.e., since the total probability is bounded between 0 and 1, the CDF is a curve whose endpoints are 0 and 1. The path which connects the endpoints solely depends on the probability distributions of the observable in question. Of course, if the signal and background share the exact same distribution, then their respective CDF curves will overlap, and any deviation between these curves is attributable to the difference between the signal and the background as they pertain to the observable in question. This informs us that the area enclosed by the region *between* the CDF curves of the signal and the background gives a reliable measure of their separation. Calculating the AP in the occupancy percentage in the observable canvas is important. The canvas for the observable starts from the bin with the first nonzero value and ends in the bin where both signal and background CDFs converge to one. For example, in Figure 2, we display the probability distribution of the pseudorapidity η of one of the leptons for both the signal and the background on the left and the corresponding CDF on the right. While the domain assigned to the probability distribution is -8 to $+8$, in the calculation of the AP, we only consider the range where the distribution is non-zero which in this case corresponds to $-2.55 \leq \eta[\ell_2] \leq +2.55$. Thus, even though an overall 100 bins exist between -8 to $+8$ in Figure 2, only 32 of these are effective in discriminating signal and background. Thus, it is important to redefine the canvas of the observable before calculating the AP in order not to underestimate it.

The AP is calculated as the summation of the absolute difference between the signal CDF curve and the background CDF curve over all the histogram bins in the redefined canvas in percentage, i.e.,

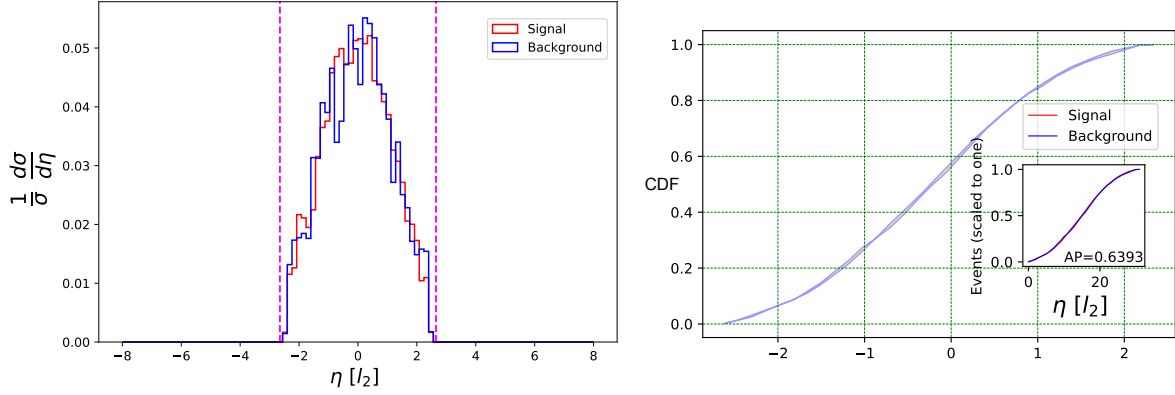


FIG. 2: (Left): The $\eta[l_2]$ distribution for the signal and background. (Right): The CDF representation of $\eta[l_2]$ observable after redefining the canvas of the $\eta[l_2]$ observable before measuring the area parameter by the omitting bins on the left and right beyond $|\eta| > 2.55$.

$$\text{AP} = \sum_{i=\text{initial bin}}^{\text{final bin}} \frac{|\text{signal}(i) - \text{background}(i)|}{\text{Number of effective bins}} * 100, \quad (14)$$

where signal (i) and background (i) are the CDF values of the signal and background curves respectively in the i^{th} bin.

In the example of $\eta[l_2]$ observable distribution in Figure 2, the right hand side plot shows the CDF path of signal and background in the inset. The AP is the percentage of area occupied by the shaded region between the signal and background CDFs and is found to be 0.6393 percent for this observable. Having thus obtained this metric for all possible observables listed in section II, our next step is to rank them based on the obtained AP values. The AP values obtained for the observables and their respective ranking over the iterations (this process will be explained shortly) are given in Table III. It is found that observable distribution $P_T(b_2)$ has the highest AP value during the first iteration, and it is ranked 1 - this row is shaded in light cyan in Table III. This observable distribution is thus highly qualified as a discriminant between signal and background and we can thus impose a cut on this variable. While this fact is indeed evident even from the normalized distribution shown in Figure 1, the AP allows us to quantify the selection based on a number, which could be more meaningful in some non-trivial selections which we will encounter in the upcoming iterations during which the signal and background curves start getting closer to each other. As another example, the AP corresponding to the observable $M(b_1, b_2, b_3, b_4, \ell_1, \ell_2)$ is calculated and displayed in Figure 3 - we can contrast this with Figure 2 to understand that this is a much better variable to put a cut on compared to $\eta[l_2]$. The AP in both cases is a measure of the shaded area between the two curves.

Having thus ranked all the observables, we will select the rank 1 observable for imposing the cut and keep the remaining observables on hold - those on hold could still be considered in the subsequent steps. At this juncture, we need to determine what exactly are the cuts to be imposed on this variable before moving to the next stage of the analysis.

B. Vertical Line Test and The Cut Choice

The conventional way of imposing cuts on an observable involves an educated guess based on what the underlying model is and where one expects the signal and background to be maximal and then by simply looking at the distributions and deciding based on their shapes. While this process certainly works, it is not guaranteed that one can identify the cut (or a set of cuts) that will certainly maximize S vs B. Herein, we seek to simply extend this method in a democratic fashion by introducing the Vertical Line Test - this involves fixing two vertical lines at the ends of the distribution and scanning the entire parameter space by changing the positions of these lines while calculating $S/\sqrt{S+B}$ for all possible cases by simply counting the signal and background events between these two vertical lines. If there are 100 bins in a histogram, then there are 4950 possible configurations of vertical lines to consider and out of these many regions, the one with the highest significance will be considered the optimal choice. While this process is certainly more computationally intensive than simply choosing one cut, it has the advantage that it can isolate

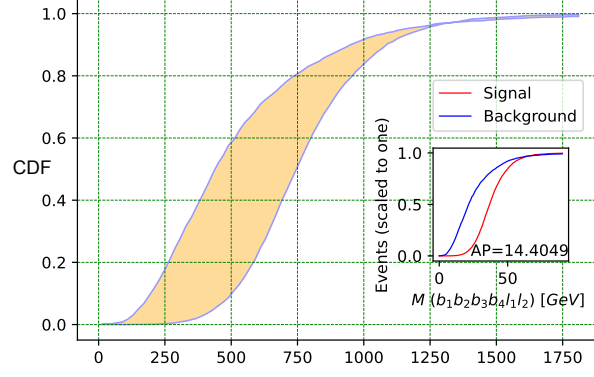


FIG. 3: The representation of the area parameter for the invariant mass $M(b_1, b_2, b_3, b_4, \ell_1, \ell_2)$ observable - the percentage of area enclosed by the shaded region is found to be 14.4049.

Variable	I1:AP	I1:Rank	I2:AP	I2:Rank	I3:AP	I3:Rank	I4:AP	I4:Rank	I5:AP	I5:Rank	I6:AP	I6:Rank	I7:AP	I7:Rank	I8:AP	I8:Rank	I9:AP	I9:Rank	I10:AP	I10:Rank	I11:AP	I11:Rank	I12:AP	I12:Rank	I13:AP	I13:Rank
$P_T(\ell_1)$	3.4558	19	7.6445	5	4.7613	15	7.9654	7	5.2735	11	7.4408	4	7.9562	4	8.4285	5	10.6837	5	15.7879	1	-	-	-	-	-	-
$P_T(\ell_2)$	1.8387	26	2.4276	20	2.4392	17	4.8515	16	2.6170	23	3.0045	19	4.7572	15	4.3527	17	4.4061	18	7.6914	9	6.5108	17	9.5743	18	12.2798	16
$P_T(b_1)$	19.7849	2	10.6604	3	11.0847	1	-	-	-	-	-	-	-	-	-	-	-	-	-	-	-	-	-	-	-	
$P_T(b_2)$	19.926	1	-	-	-	-	-	-	-	-	-	-	-	-	-	-	-	-	-	-	-	-	-	-	-	
$P_T(b_3)$	18.4332	3	11.6709	1	-	-	-	-	-	-	-	-	-	-	-	-	-	-	-	-	-	-	-	-	-	
$P_T(b_4)$	14.9833	6	11.5332	2	9.5973	3	8.7965	5	10.5614	1	-	-	-	-	-	-	-	-	-	-	-	-	-	-	-	
$\eta(\ell_1)$	1.7727	27	1.7896	28	1.5850	27	1.8382	26	2.6408	22	2.4125	20	3.4859	21	3.1426	22	3.5384	20	3.2751	19	12.1490	7	13.4533	11	17.1873	7
$\eta(\ell_2)$	0.6393	29	2.1651	27	2.5121	25	3.0584	21	3.6982	16	5.5773	8	4.5452	16	9.4437	3	14.2200	2	10.1798	4	7.7362	15	19.78581	3	18.8015	6
$\eta(b_1)$	2.5641	24	2.8338	25	3.4506	21	3.8098	19	2.7595	21	2.1799	23	3.6575	20	4.7179	16	5.1318	14	7.4179	10	5.0789	19	11.3715	12	12.4869	15
$\eta(b_2)$	2.7572	27	3.0131	24	3.3531	22	2.9788	23	2.7717	20	2.3641	22	4.3448	17	5.4369	12	6.6895	9	6.3955	15	6.0268	18	11.0038	13	13.1085	14
$\eta(b_3)$	2.7704	21	4.1736	21	4.1552	19	5.8124	13	6.0506	10	5.2712	10	6.7099	8	6.2776	9	7.2260	8	7.3627	12	9.9841	13	13.8770	10	14.2997	12
$\eta(b_4)$	2.0973	25	3.0268	23	3.3432	23	3.0476	22	2.9185	18	2.0568	24	2.8147	22	6.4267	8	12.492446	3	6.4392	14	10.1513	12	10.23958	15	17.1458	8
$\Delta R(\ell_1, \ell_2)$	2.6812	23	2.7368	26	2.306	26	3.2969	20	2.9165	19	5.1353	11	5.6793	11	9.2557	4	10.8687	4	7.9630	8	9.6058	14	8.619	17	16.635964	9
$\Delta R(b_1, b_2)$	5.2922	14	4.0122	22	4.1821	18	3.8696	18	3.9371	14	4.7852	14	2.5448	23	3.1744	21	2.8608	21	4.5335	17	12.1024	8	15.3757	7	14.5872	11
$\Delta R(b_1, b_3)$	5.0839	15	7.6405	6	9.1605	4	10.3103	2	8.7276	2	6.2754	6	8.2992	1	-	-	-	-	-	-	-	-	-	-	-	-
$\Delta R(b_1, b_4)$	4.4427	16	6.2255	11	6.0506	9	6.7451	9	4.8157	13	3.9598	16	5.4669	13	3.9861	20	5.72208	13	7.4076	11	11.7959	9	14.021	9	31.5556	1
$\Delta R(b_2, b_3)$	7.0265	13	9.0996	4	10.2425	2	9.9622	3	7.8567	5	6.7063	5	6.8646	7	11.5617	2	14.2327	1	-	-	-	-	-	-	-	-
$\Delta R(b_2, b_4)$	4.3683	17	6.1097	12	7.2161	6	5.3145	14	3.7874	15	3.1989	18	4.1116	18	5.5455	10	6.0994	11	8.104	6	10.3248	11	26.2545	1 ^a	19.30061	5
$\Delta R(b_3, b_4)$	3.4808	18	5.0145	18	5.5514	14	8.2139	6	8.4505	3	7.8622	2	8.1999	3	12.0685	1	-	-	-	-	-	-	-	-	-	-
HT	18.1399	4	5.5613	15	4.0631	20	2.0691	25	2.3955	24	4.0386	15	5.9789	10	4.7233	15	6.1947	10	12.249	2	26.8831	1	-	-	-	-
E_T	1.2848	28	4.4315	19	4.7613	15	7.1780	8	8.3040	4	10.9562	1	-	-	-	-	-	-	-	-	-	-	-	-	-	
$M(\ell_1, \ell_2)$	2.6948	22	6.2485	10	6.2472	8	6.3680	10	4.8227	12	3.7292	17	5.4738	12	4.1837	19	4.7823	15	8.1970	5	7.67783	16	7.67783	18	12.1431	17
$M(b_1, b_2)$	16.4123	5	5.0472	17	5.5639	13	4.0416	17	6.3140	8	7.4975	3	5.2162	14	5.1327	13	4.6981	16	6.1783	16	10.6855	10	10.6856	14	20.3340	4
$M(b_1, b_3)$	12.2973	8	5.8457	14	5.9564	10	9.0154	4	6.7454	6	5.0455	12	6.9125	6	4.2423	18	4.2836	19	3.3197	18	17.3150	3	17.3153	4	26.6355	3
$M(b_1, b_4)$	10.9973	9	6.5876	8	6.2481	7	6.2046	10	6.1095	9	5.9885	7	8.2203	2	7.1501	7	8.2154	7	8.0976	7	17.1870	4	17.1874	5	29.8636	2
$M(b_2, b_3)$	10.6866	10	6.0868	13	5.8493	11	6.2133	11	3.5982	17	5.0269	13	6.0490	9	5.4801	11	6.0121	12	7.3375	13	15.609	5	15.609	6	13.7946	13
$M(b_2, b_4)$	10.6865	11	6.3868	9	5.7044	12	5.2750	15	6.3882	7	5.3403	9	7.5087	5	7.6742	6	9.1676	6	10.6203	3	21.5740	2	21.5745	2	-	-
$M(b_3, b_4)$	14.4049	12	5.3241	16	3.1439	24	2.3885	24	1.6807	25	2.3847	21	3.7602	19	4.8226	14	4.4014	18	3.0099	20	14.4593	6	14.4593	8	16.00541	10
$M(bbbbbb)$	10.2528	7	6.8256	7	8.5062	5	11.6414	1	-	-	-	-	-	-	-	-	-	-	-	-	-	-	-	-	-	

^a Here, the rank 1 variable did not improve beyond the bare minimum and was kept in hold, subsequently allowing the next higher-ranked variable to be selected.

TABLE III: The AP values of the listed 29 variables and their rankings at each iteration.

the most interesting region of phase space in cases where one cannot isolate obvious bumps or other features in the distributions thus providing a neat handle on the hunt for new physics. While doing the test, it is also important to keep sufficient number of signal events while focusing on maximum significance - we have imposed the condition that the number of signal events should be a minimum of 10.⁵ In the present case, the observable $P_T(b_2)$ turns out to have rank one during Iteration 1, and the suggestion from the optimization method is to apply a selection cut on the region between the vertical lines at 130 and 990 - this is displayed in Figure 4. Having thus imposed a cut on this kinematic variable, we will drop it from further analysis - as can be seen from Table III, $P_T(b_2)$ has served its purpose at the stage of the first iteration.

⁵ This number can, of course be modified depending on the nature of the phenomenological search.

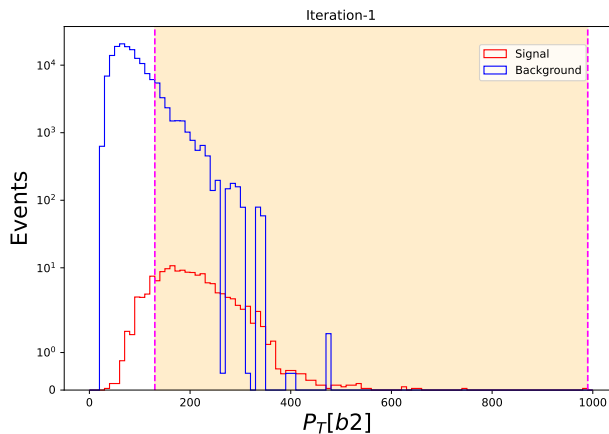


FIG. 4: Vertical line test carried over the rank 1 $P_T(b_2)$ observable during the first iteration - the suggested selection cut is shown between the two dashed lines.

Given that one would typically need multiple cuts on the events to isolate the signal from the background to effect a discovery process, the next step is to continue this process. Herein, one needs to address the question raised in the introduction to this article: in general, cutting portions of phase space will affect the distributions of the other kinematic variables as well and one needs to be cognizant of the fact that decisions on suitable cuts of these variables based on the shapes of original distributions might not be optimal anymore.⁶ While a detailed study of the correlations between all possible observables is beyond the scope of this article, we adopt the simple solution of recalculating the distributions and the associated AP of all the variables after the first cut has been imposed. This is reflected in the column “Iteration 2” in Table III for the example at hand. It is seen from that table that the variable exhibiting the next highest degree of separation as dictated by the area parameter is $P_T(b_3)$. We then run the vertical line test for this observable and design a suitable cut on it. In the next section, we summarize the methodology of this iterative process.

C. Iterations and The Cut Flowchart

Having thus imposed a cut on the second observable, our significance is likely to change. While we could simply progress to the next step, herein we introduce a choice: the decision on whether or not to include this observable in our phenomenological studies depends on how much the significance has changed. If, for example, the significance comes down, this step is not of much use. If the significance does increase but not by a lot, we again have the freedom to either use or disregard this observable. In this work, we follow the (admittedly subjective) criterion that if the significance at any particular step, say $\sigma(k)$, is greater than the previous step $\sigma(k-1)$ by 0.10, i.e., if $\sigma(k) > \sigma(k-1) + 0.10\sigma$, then that particular selection cut is accepted and we drop that observable from further analysis. This condition is adaptive to the analysis of our interest. In general, the condition can be formulated as $\sigma(k) > \sigma(k-1) + \Delta\sigma$. This condition is imposed to ensure a bare minimum improvement in each step of the algorithm for faster convergence towards a 5σ discovery potential. For this analysis, we have taken $\Delta\sigma = 0.10$ and applied a selection cut based on the satisfaction of this condition. Any other value could have been chosen - however, there is a risk that the algorithm may get stuck if none of the observables in the ranking order provide a selection cut suggestion that satisfies the bare minimum condition if it is chosen too high. In such a scenario, it is adaptive to choose a lower value of $\Delta\sigma$ to continue the progression of the methodology. In addition, we also require that if $\sigma(k) \geq 5\sigma$ for any k , the analysis stops at that point as the desired significance is reached (we call this the Lower Limiting Condition or the LL condition in what follows).

If, on the other hand, the significance at step k is such that $\sigma(k) < \sigma(k-1) + 0.10$, then we conclude that the significance has not improved much from the suggested cut from the vertical line test and so we keep that particular observable in hold (as it might well become important down the line in the analysis). We then proceed with the analysis picking the next variable with the highest AP. To understand the algorithm visually, it might be useful to represent the methodology as a flowchart that summarizes it in its entirety - this is shown in Figure 5. The different components in the flowchart are magnified in Figure 6.

⁶ We stress here that these cuts might still *work*, i.e., they might further refine the S/\sqrt{B} , however our point here is that they might not necessarily be the *optimal* ones to choose.

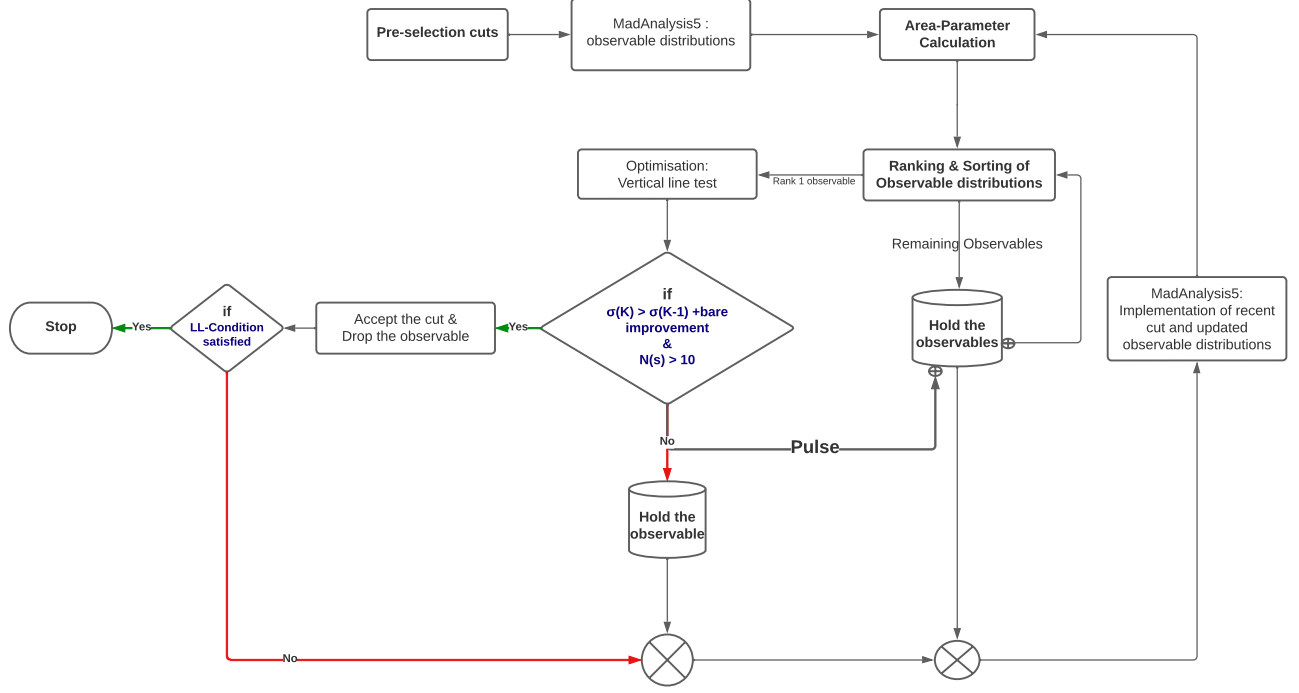


FIG. 5: A flowchart representation of the proposed algorithm.

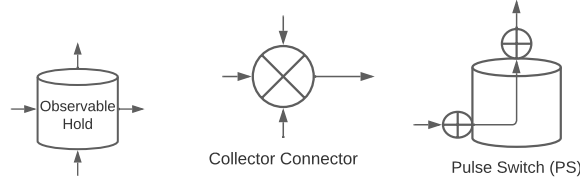


FIG. 6: The three important components in the flowchart.

Below, we summarize the features of this flowchart as a way to recap of the essential features of the proposed algorithm.

1. The generated signal and background events (after the imposition of the preselection cuts) are fed into MadAnalysis 5 and the distributions of the various kinematic observables are obtained.
2. The Area Parameter is calculated for all observables and this is then used to sort them. The observable with the highest rank is passed on to the stage of vertical line test that enables us to come up with the optimal cuts.
3. **Observable hold:** This representation showcases where we hold the remaining observable distributions for future iterations.
4. If, after the imposition of the cut, enough signal events remain ($N_s > 10$) and if an improvement in significance is obtained, the cut is accepted and the observable is dropped from further consideration. In addition, if after this cut, we satisfy the LL condition (i.e., significance becomes 5σ or higher), the process terminates.
5. If, after the imposition of the cut the LL condition is not satisfied, we pass on to the **Collector Connector (CC)**: It takes the observable distributions from the hold and pushes it to the next step. Once a proper instruction (indicated by an arrow) hits the CC, it will collect all the observable distribution sets from the hold connected to it and then recalculate all the distributions using MadAnalysis 5, calculate the AP and then sort the observables as explained previously.

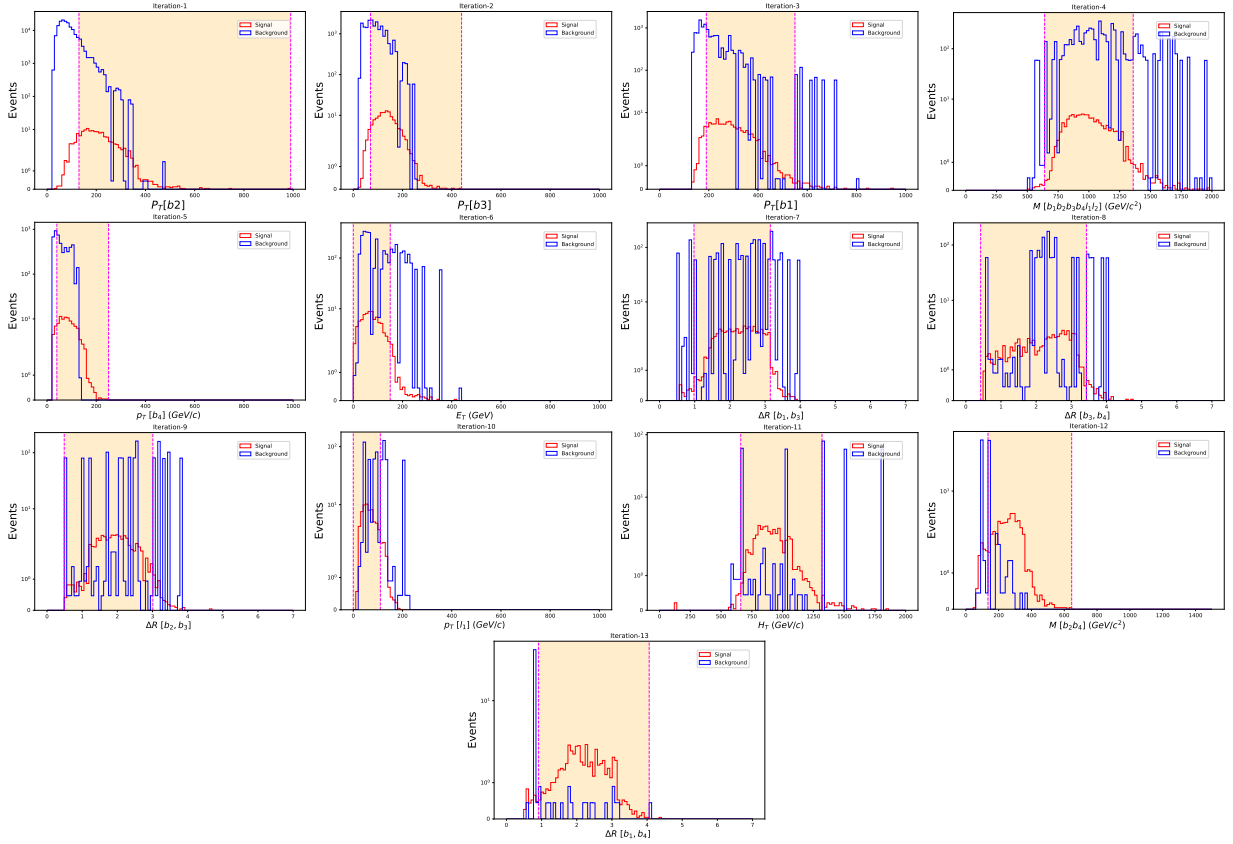


FIG. 7: The cutflow suggestions from each iteration as dictated by the vertical line test.

6. **Pulse Switch (PS):** This is an instantaneous switch that triggers the execution of an instruction when a specific condition is met (typically an ‘if’ condition in the program to check the minimum significance criterion). Otherwise, it remains inactive. Specifically, if it turns out that $\sigma(k) < \sigma(k-1) + 0.10$, then that particular observable will be sent to hold, and a pulse will activate the switch, which is connected to another hold with remaining variables. This action will make all the remaining observables in the hold go through the sorting based on ranking, followed by optimization via vertical line test on the rank-1 observable.⁷
7. The same steps continue until we either run out of observables for ranking or when the LL conditions are satisfied, i.e., the significance improved beyond 5σ . The suggested cuts on following the algorithm at each iteration are shown in [Figure 7](#) and the final cut flow chart is shown in [Table IV](#).

At this point, it would be reasonable to ask if an iterative process is indeed needed, and whether one can just use the AP designed initially and rank the variables and put in cuts as suggested by the vertical line test. This would certainly be computationally less extensive. In [Table V](#), we display the cut flow chart after applying the cuts suggested by the vertical lines test to the top 13 ranked variables from the first iteration. It is evident that the desired level of significance or effective rejection of background events has not yet been achieved (while simultaneously maintaining the essential conservation of the signal events). In contrast, using the iterative method clearly demonstrates significant improvements in the analysis, facilitating both signal conservation and background rejection concurrently as shown in [Table IV](#). The main reason for the superiority of the cutflow chart shown in [Table IV](#), which is obtained from the algorithm, is that at each iteration, MadAnalysis 5 takes into account the distributions of every observable that is modified due to an imposed threshold or selection cut on a particular observable suggested at that point in the

⁷ This particular scenario was encountered in Iteration-12 in our example.

-	Rank	-	N_{signal}	N_{BG}	σ	$\Delta\sigma$	Accepted	Z
-		initial	158.8	153612	0.405	-	-	0.010
I-1	1	$130 < PT(b_2) < 990$	135.6	20044	0.954	0.549	✓	0.067
I-2	1	$70 < PT(b_3) > 440$	126.3	13106	1.098	0.144	✓	0.096
I-3	1	$190 < PT(b_1) < 550$	111.4	7045.6	1.317	0.219	✓	0.156
I-4	1	$640 < M(\ell, \ell, b, b, b, b) < 1360$	102.8	4888.2	1.455	0.138	✓	0.207
I-5	1	$40 < PT(b_4) < 250$	91.40	3284.7	1.573	0.118	✓	0.272
I-6	1	$0 < \cancel{E}_T < 150$	83.73	2088.2	1.797	0.224	✓	0.387
I-7	1	$0.979 < \Delta R(b_1, b_3) < 3.149$	77.33	1351.4	2.046	0.249	✓	0.542
I-8	1	$0.419 < \Delta R(b_3, b_4) < 3.429$	74.32	1047.7	2.219	0.173	✓	0.663
I-9	1	$0.489 < \Delta R(b_2, b_3) < 3.01$	70.0	643.6	2.619	0.400	✓	0.979
I-10	1	$0 < PT(\ell_1) < 110$	62.26	333.3	3.130	0.511	✓	1.555
I-11	1	$660 < H_T < 1320$	58.82	132.9	4.247	1.117	✓	3.020
I-12	1	$1.470 < \Delta R(b_2, b_4) < 4.270$	45.18	69.21	4.224	-0.023	×	-
"	2	$135 < M(b_2, b_4) < 645$	51.63	69.59	4.689	0.442	✓	4.118
I-13	1	$0.9100 < \Delta R(b_1, b_4) < 4.060$	48.40	8.04	6.440	1.751	✓	10.205

TABLE IV: The final cutflowchart from the analysis as dictated by the algorithm.

-	-	N_{signal}	N_{BG}	σ	Z
-	initial	158.8	153612	0.405	0.010
R-1	$130 < PT(b_2) < 990$	135.6	20044	0.954	0.067
R-2	$200 < PT(b_1) > 700$	116.9	10660	1.126	0.108
R-3	$80 < PT(b_3) < 440$	104.2	5685.1	1.370	0.180
R-4	$740 < H_T < 1940$	96.84	5248.8	1.324	0.181
R-5	$315 < M(b_1, b_2) < 1380$	92.44	4719.3	1.333	0.192
R-6	$30 < PT(b_4) < 290$	88.82	4012.3	1.387	0.217
R-7	$720 < M(\ell, \ell, b, b, b, b) < 1640$	86.21	3490.6	1.441	0.241
R-8	$255 < M(b_1, b_3) < 765$	79.07	2707.5	1.498	0.284
R-9	$195 < M(b_1, b_4) < 510$	67.78	2049.2	1.473	0.319
R-10	$195 < M(b_2, b_3) < 585$	60.90	1266.7	1.671	0.455
R-11	$195 < M(b_2, b_4) < 575$	45.56	484.2	1.979	0.833
R-12	$90 < M(b_3, b_4) < 855$	41.64	483.4	1.817	0.764
R-13	$0.7699 < \Delta R(b_2, b_3) < 3.2199$	40.81	483.4	1.780	0.749

TABLE V: The cutflow chart for the same process following a sophisticated conventional cut and count method - we simply choose the observables that can best alienate the signal from BG from Ranking scheme and apply cuts in a sequential fashion using vertical line test.

iteration. Thus, MadAnalysis 5 reconsiders the correlation of observables at each step, recalculates distributions, and adjusts for the effects of the imposed cuts. On the other hand, Table V, although it considers the most important observables at the start of the first iteration, cannot account for the correlations among observables. As a result, many of the subsequent cuts either become redundant or negatively affect the significance. On comparing Table IV, which presents the final cutflow chart obtained from the algorithm, with Table V, which follows a sophisticated conventional cut-and-count approach, the improvement in significance over iterations demonstrates that the cut-and-count scheme applied by the algorithm is far superior. It is found that a 5σ discovery potential is achievable by following the algorithm, whereas the significance of the conventional method hovers around 1σ . A graphical representation of this comparison is provided in Figure 8.

Additionally, an important revelation from the methodology discussed is that, during the initial iteration, the observable \cancel{E}_T was positioned at the 28th out of 29 observables, making its status as one of the least preferred observables which is to be selected for vertical line test. This aligns with its low preference in the first intuition within a conventional cut and count methodology. As illustrated in Table III, the rank of \cancel{E}_T based on **AP** improves with each iteration, and in its selection eventually as the top-ranked observable in the sixth iteration. Subsequently, the vertical line test was applied to propose a selection cut. This exemplifies how constraining one observable can impact on the other observables. The selection cuts preceding \cancel{E}_T have exhibited positive effects, leading to incremental improvements in its rank based on **AP** at each step. The evolution of observable \cancel{E}_T across iterations is detailed in

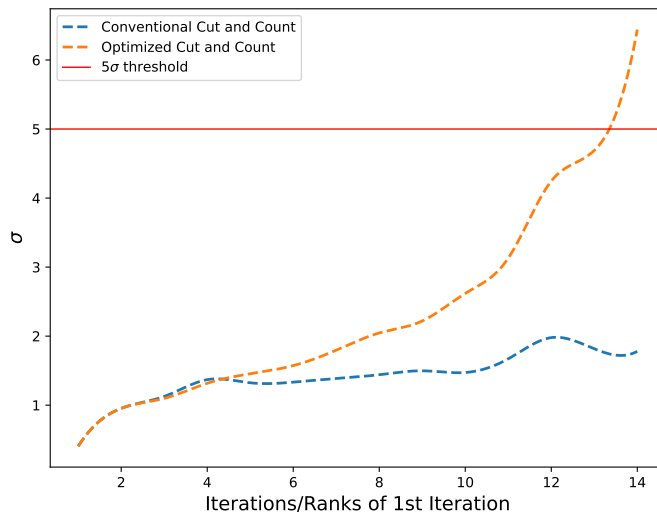


FIG. 8: Comparison of the improvement in significance between the conventional cut-and-count method applied sequentially to the top-ranked observables (Table V) and the optimized cut-and-count results obtained via the designed algorithm (Table IV).

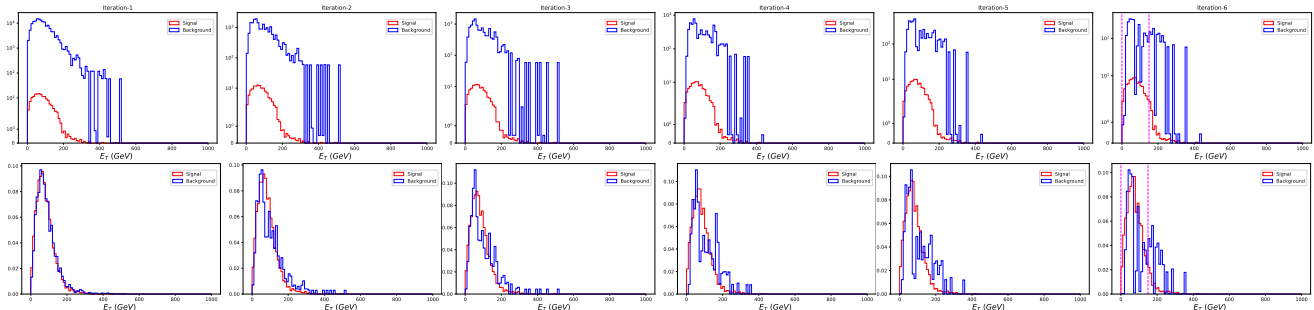


FIG. 9: Transition of E_T in the Event-Bin space (top-row) and the transition in the normalised distribution (bottom-row) from Iteration-1 to Iteration-6

Figure 9, highlighting its constraint by the vertical line test in the sixth iteration -an achievement not attainable in a typical conventional cut-based study.

IV. DISCUSSION AND CONCLUSION

Particle physics is in the midst of an exciting time - while the searches at the LHC for hints of BSM physics have not borne fruit thus far, it is nevertheless a very interesting question to ask how much and how far one could probe models with more refined and sophisticated techniques in order to help discover the expected new TeV scale physics. While the ML and other computational techniques are apt for this purpose, our motivation here is slightly different - the traditional cut and count method of doing phenomenological analysis has been enormously successful and has stood the test of time thus far. Thus, it is interesting to ask if one could keep the spirit of this approach while trying to optimize this strategy for better results. This can also yield results that are phenomenologically interpretable, unlike deep neural networks, which cannot explain why their parameters can perfectly execute the assigned task, leading to what we refer to as the black-box nature.

In this spirit, we demonstrated in this paper that one could use a cut-based strategy to uncover new physics but with a more systematic and streamlined approach. Our analysis starts by ranking all observables associated with any given new physics process on the basis of the newly introduced Area Parameter - a metric that looks for maximum signal-background separation. Having ranked the observables, we employ the Vertical Line Test to systematically isolate the region of phase space that yields the maximum significance. The process is then iterated over the other observables yielding a final significance that can supercede the one obtained by conventional techniques.

In our analysis, we considered a process featuring a pair of charged Higgs particles decaying into W^+W^- , accompanied by a pair of two pseudoscalar particles undergoing subsequent decays into $b\bar{b}$. This results in a final state topology that is rather complex and challenging, thus providing an excellent platform for evaluating the effectiveness of the proposed algorithm. Contrasted with the traditional cut-and-count method, we demonstrated that our current algorithm performs significantly better in terms of isolating the signal from the background, giving us a significance of more than 5σ while the traditional cut and count methodology for this same final state yields only around 1σ . However, this does come at a price - it entails a notably higher level of computational complexity and thus, total computational time. This increased complexity stems primarily from the dynamic nature of observable rankings, which change with each iteration as we isolate different regions of phase space. As a consequence, the background execution of MadAnalysis 5 is necessary to compute the CDFs related to the observables after each iteration. Nonetheless, we expect that this might be less important than achieving a superior searching technique, particularly for new physics signals that might involve complicated final states.

V. ACKNOWLEDGEMENTS

BC acknowledges support from the Department of Science and Technology, India, under Grant CRG/2020/004171. GBK is supported by the Prime Minister's Research Fellowship (Grant No: PMRF-192002-1802) from the Department of Science and Technology, India. AS acknowledges the monetary support which is received from Anusandhan National Research Foundation (ANRF) through the SERB-NPDF grant (Ref No: PDF/2023/002572). The work of S.S. is supported by Fundação de Amparo à Pesquisa do Estado de São Paulo (FAPESP) grant 2021/09547-9.

VI. DATA AVAILABILITY STATEMENT

Datasets developed for the project can be made available upon reasonable request. Considering the volume of data generated using the Monte Carlo simulation for the project, a list of generated processes can also be an alternative to reproducing the result.

-
- [1] S. L. Glashow, "Partial Symmetries of Weak Interactions," *Nucl. Phys.* **22**, 579–588 (1961).
 - [2] Steven Weinberg, "A Model of Leptons," *Phys. Rev. Lett.* **19**, 1264–1266 (1967).
 - [3] Abdus Salam, "Weak and Electromagnetic Interactions," *Conf. Proc. C* **680519**, 367–377 (1968).
 - [4] Dan Guest, Kyle Cranmer, and Daniel Whiteson, "Deep Learning and its Application to LHC Physics," *Ann. Rev. Nucl. Part. Sci.* **68**, 161–181 (2018), [arXiv:1806.11484 \[hep-ex\]](#).
 - [5] Luke de Oliveira, Michael Kagan, Lester Mackey, Benjamin Nachman, and Ariel Schwartzman, "Jet-images — deep learning edition," *JHEP* **07**, 069 (2016), [arXiv:1511.05190 \[hep-ph\]](#).
 - [6] J. Alwall, R. Frederix, S. Frixione, V. Hirschi, F. Maltoni, O. Mattelaer, H. S. Shao, T. Stelzer, P. Torrielli, and M. Zaro, "The automated computation of tree-level and next-to-leading order differential cross sections, and their matching to parton shower simulations," *JHEP* **07**, 079 (2014), [arXiv:1405.0301 \[hep-ph\]](#).
 - [7] Adam Alloul, Neil D. Christensen, Céline Degrande, Claude Duhr, and Benjamin Fuks, "FeynRules 2.0 - A complete toolbox for tree-level phenomenology," *Comput. Phys. Commun.* **185**, 2250–2300 (2014), [arXiv:1310.1921 \[hep-ph\]](#).
 - [8] Torbjörn Sjöstrand, Stefan Ask, Jesper R. Christiansen, Richard Corke, Nishita Desai, Philip Ilten, Stephen Mrenna, Stefan Prestel, Christine O. Rasmussen, and Peter Z. Skands, "An introduction to PYTHIA 8.2," *Comput. Phys. Commun.* **191**, 159–177 (2015), [arXiv:1410.3012 \[hep-ph\]](#).
 - [9] J. de Favereau, C. Delaere, P. Demin, A. Giammanco, V. Lemaître, A. Mertens, and M. Selvaggi (DELPHES 3), "DELPHES 3, A modular framework for fast simulation of a generic collider experiment," *JHEP* **02**, 057 (2014), [arXiv:1307.6346 \[hep-ex\]](#).
 - [10] Eric Conte, Benjamin Fuks, and Guillaume Serret, "MadAnalysis 5, A User-Friendly Framework for Collider Phenomenology," *Comput. Phys. Commun.* **184**, 222–256 (2013), [arXiv:1206.1599 \[hep-ph\]](#).
 - [11] Kyle Cranmer, Juan Pavez, and Gilles Louppe, "Approximating Likelihood Ratios with Calibrated Discriminative Classifiers," (2015), [arXiv:1506.02169 \[stat.AP\]](#).
 - [12] Pierre Baldi, Kyle Cranmer, Taylor Faucett, Peter Sadowski, and Daniel Whiteson, "Parameterized neural networks for high-energy physics," *Eur. Phys. J. C* **76**, 235 (2016), [arXiv:1601.07913 \[hep-ex\]](#).
 - [13] Amit Chakraborty, Sung Hak Lim, and Mihoko M. Nojiri, "Interpretable deep learning for two-prong jet classification with jet spectra," *JHEP* **07**, 135 (2019), [arXiv:1904.02092 \[hep-ph\]](#).
 - [14] Taylor Faucett, Jesse Thaler, and Daniel Whiteson, "Mapping Machine-Learned Physics into a Human-Readable Space," *Phys. Rev. D* **103**, 036020 (2021), [arXiv:2010.11998 \[hep-ph\]](#).

- [15] Aishik Ghosh, Benjamin Nachman, and Daniel Whiteson, “Uncertainty-aware machine learning for high energy physics,” *Phys. Rev. D* **104**, 056026 (2021), [arXiv:2105.08742 \[physics.data-an\]](#).
- [16] Sven Bollweg, Manuel Haußmann, Gregor Kasieczka, Michel Luchmann, Tilman Plehn, and Jennifer Thompson, “Deep-Learning Jets with Uncertainties and More,” *SciPost Phys.* **8**, 006 (2020), [arXiv:1904.10004 \[hep-ph\]](#).
- [17] G. C. Branco, P. M. Ferreira, L. Lavoura, M. N. Rebelo, Marc Sher, and Joao P. Silva, “Theory and phenomenology of two-Higgs-doublet models,” *Phys. Rept.* **516**, 1–102 (2012), [arXiv:1106.0034 \[hep-ph\]](#).
- [18] Anirban Karan, Víctor Miralles, and Antonio Pich, “Global fit of the Aligned Two-Higgs-Doublet Model,” in *2023 European Physical Society Conference on High Energy Physics* (2023) [arXiv:2312.00514 \[hep-ph\]](#).
- [19] Heather E. Logan, “TASI 2013 lectures on Higgs physics within and beyond the Standard Model,” (2014), [arXiv:1406.1786 \[hep-ph\]](#).
- [20] Majid Hashemi and Laleh Roushandel, “Charged Higgs decay to $W^\pm H$ at a high energy lepton collider,” (2023), [arXiv:2310.06519 \[hep-ph\]](#).
- [21] Georges Aad *et al.* (ATLAS), “Search for charged Higgs bosons decaying via $H^\pm \rightarrow \tau^\pm \nu$ in fully hadronic final states using pp collision data at $\sqrt{s} = 8$ TeV with the ATLAS detector,” *JHEP* **03**, 088 (2015), [arXiv:1412.6663 \[hep-ex\]](#).
- [22] Vardan Khachatryan *et al.* (CMS), “Search for a charged Higgs boson in pp collisions at $\sqrt{s} = 8$ TeV,” *JHEP* **11**, 018 (2015), [arXiv:1508.07774 \[hep-ex\]](#).
- [23] Georges Aad *et al.* (ATLAS), “Search for charged Higgs bosons in the $H^\pm \rightarrow tb$ decay channel in pp collisions at $\sqrt{s} = 8$ TeV using the ATLAS detector,” *JHEP* **03**, 127 (2016), [arXiv:1512.03704 \[hep-ex\]](#).
- [24] Debtosh Chowdhury and Otto Eberhardt, “Update of Global Two-Higgs-Doublet Model Fits,” *JHEP* **05**, 161 (2018), [arXiv:1711.02095 \[hep-ph\]](#).
- [25] Glen Cowan, Kyle Cranmer, Eilam Gross, and Ofer Vitells, “Asymptotic formulae for likelihood-based tests of new physics,” *Eur. Phys. J. C* **71**, 1554 (2011), [Erratum: *Eur.Phys.J.C* 73, 2501 (2013)], [arXiv:1007.1727 \[physics.data-an\]](#).
- [26] Li-Gang Xia, “QBDT, a new boosting decision tree method with systematical uncertainties into training for High Energy Physics,” *Nucl. Instrum. Meth. A* **930**, 15–26 (2019), [arXiv:1810.08387 \[physics.data-an\]](#).
- [27] A. Bhattacharyya, “On a measure of divergence between two multinomial populations,” *Sankhyā: The Indian Journal of Statistics (1933-1960)* **7**, 401–406 (1946).
- [28] S. Kullback and R. A. Leibler, “On information and sufficiency,” *The Annals of Mathematical Statistics* **22**, 79–86 (1951).